Transportation Research Part C 93 (2018) 322–334

Contents lists available at ScienceDirect

Transportation Research Part C

journal homepage: www.elsevier.com/locate/trc

Distributed conflict-free cooperation for multiple connected vehicles at unsignalized intersections

Biao Xu[a], Shengbo Eben Li[a], Yougang Bian[a], Shen Li[b], Xuegang Jeff Ban[c], Jianqiang Wang[a], Keqiang Li[a,*]

[a] State Key Laboratory of Automotive Safety and Energy, Tsinghua University, Beijing 100084, China
[b] Department of Civil and Environmental Engineering, University of Wisconsin-Madison, Madison 53706, USA
[c] Department of Civil and Environmental Engineering, University of Washington, Seattle 98105, USA

ARTICLE INFO

Keywords:
Connected and automated vehicle
Cooperative control
Unsignalized intersection
Virtual platoon

ABSTRACT

Connected vehicles will change the modes of future transportation management and organization, especially at intersections. In this paper, we propose a distributed conflict-free cooperation method for multiple connected vehicles at unsignalized intersections. We firstly project the approaching vehicles from different traffic movements into a virtual lane and introduce a conflict-free geometry topology considering the conflict relationship of involved vehicles, thus constructing a virtual platoon. Then we present the modeling of communication topology to describe two modes of information transmission between vehicles. Finally, a distributed controller is designed to stabilize the virtual platoon for conflict-free cooperation at intersections. Numerical simulations validate the effectiveness of this method.

1. Introduction

The increasing demand for mobility poses great challenges to road transport. The cyber-connection of automated vehicles is attracting extensive attention, due to its potential to benefit traffic safety and efficiency. A group of connected and automated vehicles (CAV) is actually a multi-agent system with three layered and interrelated dynamics. In the bottom layer, vehicle dynamics contains both continuous-time systems, e.g., engine, tire, aerodynamic drag, etc., and event-driven discrete-time systems, e.g., gear shifting, hybrid powertrain mode switching, etc. In the middle layer, all vehicles in the traffic flow are constrained by both road geometry, e.g., road shape and structure, and traffic management, e.g., traffic light and speed limit. In the top layer, cyber-communication is strongly intertwined with the other two layers, and has such issues as topological variety, packet loss, time-delay, etc. Such a layered multi-agent system is dynamically coupled at the bottom, tempo-spatially constrained in the middle, and topologically interacted in a large scale on the top, which poses remarkable challenges to the behavioral harmonization for multiple vehicles with longitudinal and lateral dimensions.

The widely studied, but also simplified, version of connected vehicle cooperation is the platoon control system in highways. Platoon control aims to ensure that a group of connected vehicles in the same lane move at a harmonized longitudinal speed, while maintaining desired inter-vehicle spaces. Typically, a platoon can be considered as a one-dimensional multi-agent system in the formation of either open-chain or cyclic geometry. According to the system decomposability, platoon control methods can be categorized into two types, i.e., cascading feedback design (Naus et al., 2010; Ploeg et al., 2014; Seiler et al., 2004; Xiao and Gao, 2011; Zhou and Peng, 2005) and graph-decomposition design (Fax and Murray, 2004; Lewis et al., 2013; Li et al., 2010, 2017; Wang et al.,

* Corresponding author.
E-mail address: likq@tsinghua.edu.cn (K. Li).

https://doi.org/10.1016/j.trc.2018.06.004
Received 12 December 2017; Received in revised form 3 May 2018; Accepted 10 June 2018
Available online 22 June 2018

2013; You and Xie, 2011; Zheng et al., 2016a, 2016b). In the former, each vehicle uses radar for information acquisition and adopts decentralized control strategy to keep a desired distance behind the preceding vehicle, thus the feedback loops of two successive vehicles are coupled in a cascading structure. In the latter, vehicles are interconnected by communication channels, of which the various topologies result in complex coupling in the closed-loop dynamics.

For the cascading feedback design, the string stability must be enforced to eliminate any rear-end collisions, i.e., the spacing errors should not be amplified along the platoon. For example, Seiler et al. (2004) studied string stability for platoons with different topologies and found that due to the existence of complementary sensitivity integral constraint, small disturbances acting on one vehicle can propagate and have a large effect on another vehicle. Xiao and Gao (2011) took into account parasitic time delays and lags in string stability analysis. It was indicated that the negative effect of parasitic time delays on string stability is larger than that of time lags. Ploeg et al. (2014) proposed an H-infinity controller synthesis approach for L-2 string stability, which allows for the explicit inclusion of the string stability requirement. For the graph-decomposition design, such systems can be cast into a set of decoupled low-dimensional systems through graph decomposition in some special cases. For example, Fax and Murray (2004) proposed a separation principle that can decompose formation stability into two components: the stability of the information flow and the stability of the individual vehicle. Li et al. (2010) proposed a framework for the consensus of a multi-agent system, which can be cast into the stability of a set of matrices of the same low dimension. Zheng et al. (2016a) further extended the above method to a four-component framework for vehicle platoon control. A unified internal stability theorem was proved by using the algebraic graph theory and Routh–Hurwitz stability criterion.

As a typical scenario in urban areas, the intersection is more complex and challenging for multi-vehicle coordination than highway. In the intersection, vehicles enter from different intersection entrances, cross their position trajectories at the intersection zone, and leave the intersection at different exits, leading to a two-dimensional vehicle formation. The complex conflict relationship of vehicles in the two-dimensional formation results in complicated vehicle decisions to avoid collisions at the intersection. Besides, vehicle formation at an intersection has high-dimensional and discrete dynamics considering a large number of individual vehicles. Therefore, multi-vehicle coordination at intersections is quite difficult. Additionally, it was reported that 36% of the vehicle crashes were intersection-related in the USA (Choi, 2010). Hence, multi-vehicle coordination at intersections is critical to traffic safety and efficiency in urban areas (Chen and Englund, 2016). To resolve conflicts of vehicles passing an intersection, traffic signals may be present. In this case, certain design scheme such as the dual-diagram design can be applied to ensure the safety of passing vehicles. One example of this is the recent paper by Xu et al. (2017). Additionally, Goodall et al. (2013) used simulation methods to predict the queue length and delay after obtaining vehicle position and speed information via V2I, which was then used to optimize traffic signal timing. Feng et al. (2015) presented a real-time adaptive signal control algorithm using the connected vehicle data and a bi-level optimization problem was formulated to minimize the vehicle delay and queue length. These traffic signal based coordination methods for intersection control can effectively separate the conflicting traffic movements to ensure traffic safety. These methods are also feasible in the mixed traffic environment where CAVs, human-driving vehicles, and other traffic participants exist concurrently. However, the traffic signal may bring the green time loss, which results in inefficiency for intersection management. Hence, researchers have started to focus on signal-free methods for intersection coordination. Currently, most of the existing studies without the traffic signal focused on centralized coordination methods which utilize the global information of the whole intersection to centralizedly organize the motion of all approaching vehicles (Dai et al., 2016; Dresner and Stone, 2008; Huang et al., 2012; Kamal et al., 2015; Lee and Park, 2012; Lee et al., 2013; Wu et al., 2012; Zhang et al., 2015). For example, Dresner and Stone (2008) suggested a reservation-based approach in which the vehicle agent reserve a block of space-time in the intersection and the intersection arbiter agent manages the reservations according to the “First Come, First Served” policy. Similar methods can be found in Huang et al. (2012) and Zhang et al. (2015). Lee and Park (2012) created a vehicle-intersection cooperation algorithm, which optimizes the trajectories of approaching vehicles by eliminating potential overlaps of the trajectories for conflicting vehicles. Kamal et al. (2015) presented a global coordination scheme for automated vehicles at an intersection, which uses a model predictive control framework to acquire the vehicle optimal trajectories considering the cross-collision risks. Other examples can be found in Wu et al. (2012), Lee et al. (2013) and Dai et al. (2016).

The centralized coordination methods, however, need huge computation resources since they own a centralized controller to optimize the trajectories for all approaching vehicles. Additionally, each vehicle needs to communicate with the centralized controller, which results in heavy communication load and strict requirement on information security. Distributed control is an alternative solution with merits of lower computational complexity, less communication, and better information security. In distributed control, each approaching vehicle owns an individual controller to optimize the trajectory considering the motion information and the conflict relationship with its neighboring vehicles (Li and Wang, 2006; Ahmane et al., 2013). Li and Wang (2006) used safety driving patterns to represent the collision-free movements of vehicles at intersections and planed individual vehicle trajectories of the collision-free driving schedule. To select the traffic-efficient driving schedule, they adopted a binary tree to enumerate all potential driving schedules of the intersection crossing. However, the algorithm owns the complexity of exceeding O(n!), which brings a heavy calculation load. Ahmane et al. (2013) used a Timed Petri Net with Multipliers (TPNM) to discrete and represent the traffic dynamic model, and introduced the distributed clearing policy that leads to a global complex behavior. However, they just considered the going-straight traffic movements with simple conflict relationships. Actually, the traffic movements in real intersections are much more complicated, which may lead to failure of their method. To sum up, the existing distributed methods for unsignalized intersections do not fully consider the global complex conflict relationship of all approaching vehicles utilizing an algorithm with low computational complexity.

This paper presents a new distributed conflict-free cooperation method for multiple connected and automated vehicles in continuous traffic flow at unsignalized intersections. The main idea of this paper is to transform the two-dimension vehicle cluster at the

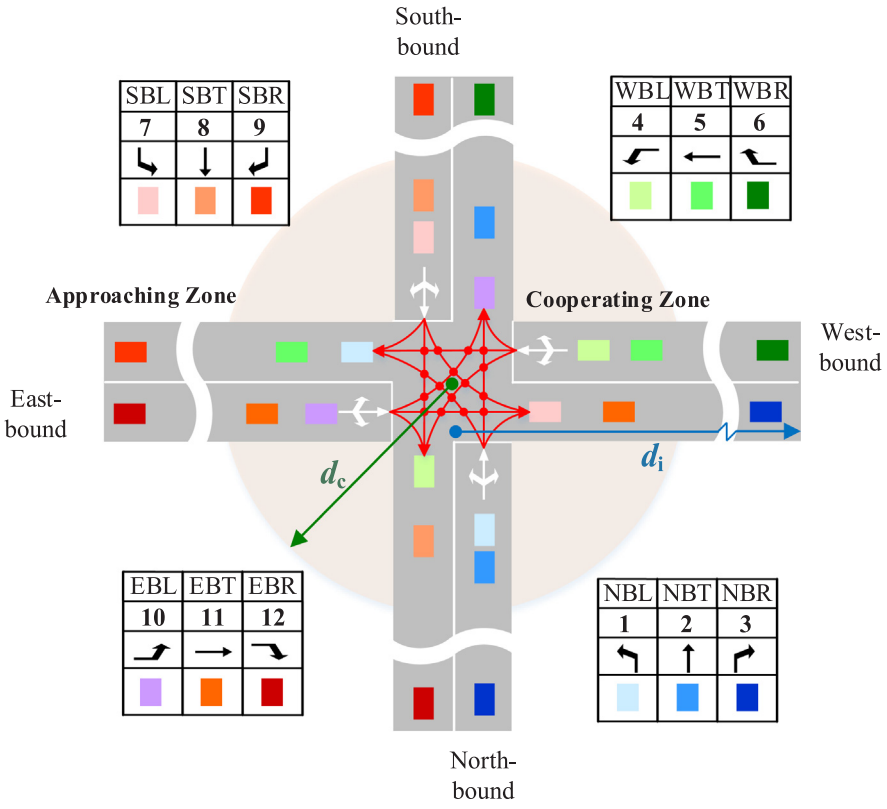

Fig. 1. Setup of the typical intersection.

intersection to one-dimension vehicle virtual platoon. To achieve it, we project vehicles from different traffic movements into a virtual lane, introduce a conflict-free geometry topology based on the conflict relationship of different traffic movements, propose a communication topology to characterize the communication structure, design the distributed feedback controller, and eventually construct a conflict-free virtual platoon system. The advantages of this method include: (1) complete consideration of the conflict relationship of all approaching vehicles; (2) low complexity to construct the conflict-free geometry topology.

2. Problem statement

We consider a typical 4-leg, 1-lane unsignalized intersection (see Fig. 1). This intersection has four entrances and four exits. Each entrance or exit is assumed to have only one lane. The vehicles from the same approaching direction will follow FIFO (first-in-first-out) and no vehicle overtaking will occur. Vehicles in each lane of the intersection entrance can turn left, go straight and turn right, forming 12 potential traffic flow movements at this intersection. The traffic movements are counterclockwise numbered with 1–12. The 12 movements are illustrated in Fig. 1, including their conflicting relationships. There are totally 16 crossing points and 4 converging points at this intersection, bringing 20 conflicting points. The conflicting vehicles cannot pass the intersection at the same time.

Additionally, the intersection is divided into two zones, i.e., approaching zone and cooperating zone (Fig. 1). The former allows vehicles in each entrance to implement car-following with their front vehicle, while the latter is dedicated to supporting vehicles at all entrances to self-organize and achieve no-conflict passing at the intersection. The radius of overall intersection is assumed to be d_i, and the radius of cooperating zone is assumed to be d_c.

We assume that all vehicles are equipped with positioning and V2V communication devices so that they can share location and movement information when they enter the cooperating zone of the intersection. Additionally, all approaching vehicles are assumed to be automated vehicles so that vehicles can strictly follow the desired acceleration, control the speed, and pass the intersection automatically. That is, we assume 100% penetration of CAV equipped vehicles in this research.

3. Methodology

3.1. Traffic movement conflict model

The complexity of intersection control lies in the conflict relationship of different traffic movements. As shown in Fig. 2, an intersection typically has four conflicting modes (Roess et al., 2011), including crossing, converging, diverging, and no conflict. The

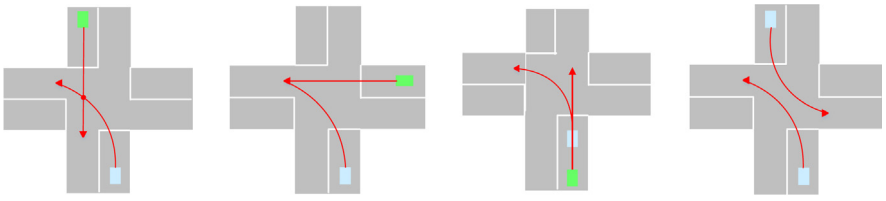

(a) Crossing (b) Converging (c) Diverging (d) No-conflict

Fig. 2. Conflict modes.

first three modes describe the conflict relationship of the traffic movements in the intersection areas, in the exit lanes, and in the entrance lanes, respectively, which are used to avoid the conflicting vehicles passing the intersection simultaneously. Additionally, each traffic movement has the diverging conflict relationship with itself according to the definition of the conflict modes.

We define that the crossing set $\mathbb{S}_k$, converging set $\mathbb{Q}_k$, and diverging set $\mathbb{R}_k$ consist of all traffic movements that have the cross relationship, converging relationship, and diverging relationship with traffic movement k, respectively. Further, conflict set $\mathbb{C}_k$ is defined as the union set of $\mathbb{S}_k$, $\mathbb{Q}_k$, and $\mathbb{R}_k$. Fig. 3 presents the conflict relationships of the traffic movements in Fig. 1 in which the dashed lines represent the converging relationship, solid lines refer to the cross relationship, and the rectangles denote the diverging relationship. Based on the conflict relationship shown in Fig. 3, we can easily obtain the conflict set $\mathbb{S}$, $\mathbb{Q}$, $\mathbb{R}$, and $\mathbb{C}$. Taking the northbound left movement (No. 1 traffic movement) as an example, $\mathbb{S}_1 = \{4, 8, 10, 11\}$, $\mathbb{Q}_1 = \{5, 9\}$, $\mathbb{R}_1 = \{1, 2, 3\}$, and $\mathbb{C}_1 = \{1, 2, 3, 4, 8, 10, 11\}$.

Note that when one traffic movement belongs to the conflict set of another traffic movement, the trajectories of the vehicles in this two traffic movement must conflict in the intersection area. In reverse, when the trajectories of two vehicles conflict in the intersection area, the traffic movement of one vehicle must belong to the conflict set of the traffic movement of the other vehicle.

3.2. Geometry topology

We project the vehicles in different traffic movements onto a virtual lane according to their distance to the intersection center, and then construct a virtual platoon (Fig. 4). The vehicles are numbered in order with $1 \sim N$ according to the distance. A virtual leading vehicle (numbered as 0) with a constant speed v_t is assigned to the virtual platoon. Here, v_t represents the safe but efficient speed for vehicles passing the intersection, and is usually a pre-set constant. When the speed of the virtual leading vehicle is determined, the following vehicles will track this speed for intersection coordination.

Notice that the virtual platoon is different from the real vehicle platoon in the sense of geometry formation and communication topology. As for the geometry formation, a vehicle in the virtual platoon may not follow its nearest preceding vehicle but one of the non-immediate preceding vehicles, which depends on the conflict relationships of vehicles. Concerning the communication topology, the virtual platoon owns distinct information transmission modes which will be described in detail in Section 3.3.

For vehicle i ($i \in \mathcal{N}^+$, $i \leqslant N$) in traffic movement S_i, the conflict vehicle set $\mathbb{P}_i$ consists of all vehicles that lie in front of vehicle i and have conflict relationship with it. Hence,

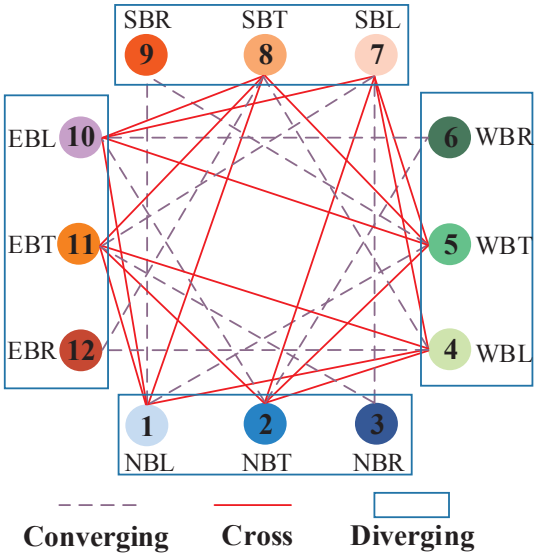

Fig. 3. Conflict relationships.

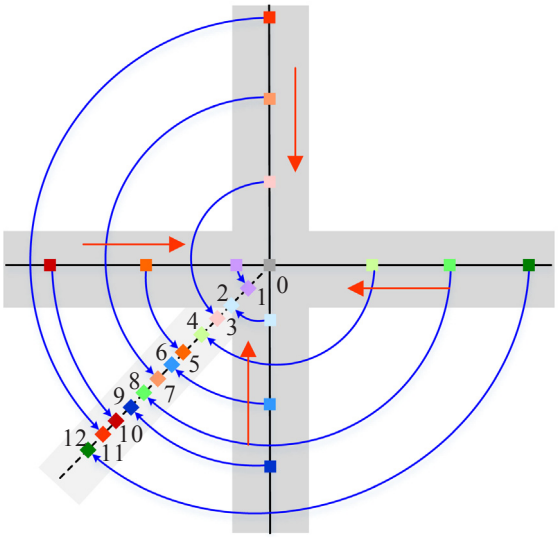

Fig. 4. Virtual platoon projection.

$$\mathbb{P}_i = \{j | j < i,\ S_j \in \mathbb{C}_{S_i},\ j \in \mathcal{N}^+\}. \tag{1}$$

Here, S_j denotes the traffic movement that vehicle j belongs to, and $\mathbb{C}_{S_i}$ denotes the union conflict set of the traffic movement S_i. Sometimes, $\mathbb{P}_i = \varnothing$, which means there is no vehicle in front of vehicle i and having conflict relationship with it. For example, $\mathbb{P}_1 = \varnothing$ in Fig. 4. In this case, let

$$\mathbb{P}_i = \{0\}, \tag{2}$$

which means that the conflict vehicle set only includes the virtual leading vehicle 0.

Take the virtual platoon in Fig. 5(a) as an example. Vehicle 1–10 belong to the No. 5, 12, 10, 9, 4, 1, 7, 6, 8, and 3 traffic movement of Fig. 1, respectively. Based on the conflict relationship described in Fig. 3 and the definition in Eqs. (1) and (2), the conflict vehicle sets of vehicle 1–vehicle 10 are $\mathbb{P}_1 = \{0\}$, $\mathbb{P}_2 = \{0\}$, $\mathbb{P}_3 = \{1, 2\}$, $\mathbb{P}_4 = \{1\}$, $\mathbb{P}_5 = \{1, 2\}$, $\mathbb{P}_6 = \{1, 3, 4, 5\}$, $\mathbb{P}_7 = \{1, 3, 4, 5\}$, $\mathbb{P}_8 = \{1, 3, 5\}$, $\mathbb{P}_9 = \{1, 2, 3, 4, 5, 6, 7\}$, and $\mathbb{P}_{10} = \{6, 7\}$.

Based on the conflict vehicle sets, we use a directed graph $\mathcal{G}_{N+1} = \{\mathcal{V}_{N+1}, \mathcal{E}_{N+1}\}$ to represent the conflict relationships of the virtual platoon. In the directed graph $\mathcal{G}_{N+1}$, the vertice set $\mathcal{V}_{N+1}(\mathcal{V}_{N+1} = \{0, 1, 2, \cdots, N\})$ represents the set of individual vehicles and the directed edge set $\mathcal{E}_{N+1}$ $(\mathcal{E}_{N+1} = \{(i, j)\ \})$ indicates the conflict relationships between vehicles, i.e., when vehicle j belongs to the conflict vehicle set $\mathbb{P}_i$ of vehicle i, we have $(j, i) \in \mathcal{E}_{N+1}$. For example, the directed graph of the virtual platoon in Fig. 5(a) is shown in Fig. 5(b).

Definition 1. If $\forall\ k \in \{2, 3, \cdots, n\}$, we have $(i_{k-1}, i_k) \in \mathcal{E}_{N+1}$, then the edge sequence $\{(i_1, i_2), (i_2, i_3), \cdots, (i_{n-1}, i_n)\}$ in the directed graph $\mathcal{G}_{N+1}$ is defined as a directed path from vertice i_1 to vertice i_n.

Then we find the depth-first spanning tree $\check{\mathcal{G}}_{N+1}$ (Tarjan, 1972) of the conflict directed graph $\mathcal{G}_{N+1}$.

Theorem 1. The directed graph constructed based on the conflict relationships have the depth-first spanning tree with the root node being vertice 0.

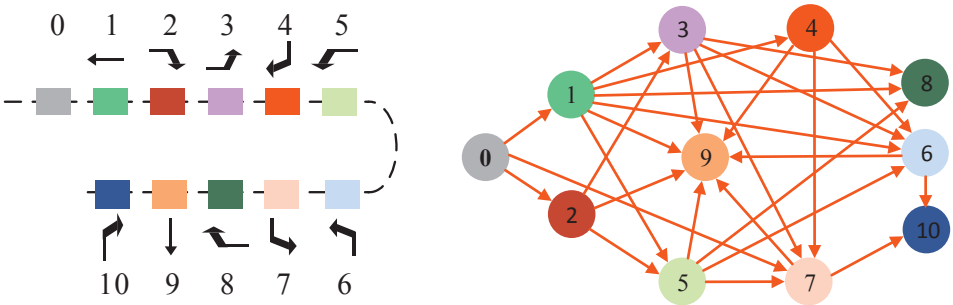

Fig. 5. An example of a projected virtual platoon and the corresponding graph.

Table 1
The proposed spanning tree algorithm.

Input: The graph $\mathscr{G}_{N+1}$.
Output: The spanning tree $\check{\mathscr{G}}_{N+1}$.

1: The depth of the vertice 0 d_0 is set to 0, i.e., $d_0 = 0$.
2: **for** $i = 1, 2, 3, \ldots, N$ **do**
3: Find all the parent vertices j of vertice i in $\mathscr{G}_{N+1}$, i.e., $j \in \{j|(j, i) \in \mathscr{E}_{N+1}\}$.
4: Find the vertice k with the largest depth d_k among the parent vertices.
5: Set the parent vertice of i as vertice k in the graph $\check{\mathscr{G}}_{N+1}$, add a vertice i and an edge (k, i) to the graph $\check{\mathscr{G}}_{N+1}$, and set the depth of the vertice i to $d_k + 1$.
6: **end for**

Proof. We prove that there exist directed paths from vertice 0 to all the other vertices $1 \sim n$ by using the mathematical induction.

(1) For vehicle 1, $\mathbb{P}_1 = \{0\}$. Hence, $(0, 1) \in \mathscr{E}_{N+1}$, i.e., there exists a directed path from vertice 0 to vertice 1.
(2) We assume that there exist directed paths from 0 to $1 \sim k$ ($k \geq 1$). For vertice $k+1$, if $\mathbb{P}_{k+1} = \{0\}$, then we have $(0, k+1) \in \mathscr{E}_{N+1}$, i.e., there exists a directed path from vertice 0 to vertice k + 1. Otherwise, there must exist a vehicle $j \in \mathbb{P}_{k+1}$ ($j < k+1$), i.e., $\exists\, j < k+1$, such that $(j, k+1) \in \mathscr{E}_{N+1}$. Since there exist directed paths from vertice 0 to vertice j ($j \leqslant k$), then there must exists a directed path from vertice 0 to vertice k + 1. That is, there exist directed paths from vertice 0 to vertice $1 \sim k+1$.

Hence, there exist directed paths from vertice 0 to all the other vertices in the directed graph $\mathscr{G}_{N+1}$. Therefore, there exists a spanning tree with root node vehicle 0, which also means there exists the depth-first spanning tree with the root node being vertice 0. □

The depth-first spanning tree can be calculated by the depth-first search algorithm, which selects the reserved edges and deletes the other edges according to the edge class. In the virtual platoon and the conflict graph, there only exist directed edges from the front vehicle vertices to the following vehicle vertices. Hence, we propose a search algorithm shown in Table 1, which considers the characteristics of the directed graph to find the spanning tree $\check{\mathscr{G}}_{N+1}$ of $\mathscr{G}_{N+1}$. Taking the directed graph in Fig. 5(b) as an example, the proposed spanning tree is shown in Fig. 6.

The search algorithm is an iterative search algorithm, which decides the depth of the vertices one by one in the order they are numbered. Actually, when the virtual platoon is generated and the spanning tree has been constructed, if a new vehicle is entering the intersection coordination area, instead of search for the spanning tree again, we just need to determine the depth and the parent vertice of the entering vehicle following step 3–5 in Table 1. Hence, the computation load can be decreased.

In the spanning tree, we can define the ancestor and descendent set $\mathbb{A}_i$ and the set of the vertices with the same depth $\mathbb{B}_i$ of vertice i. The former consists of all ancestor vertices and descendent vertices of vertice i, and the latter consists of all the vertices which have the same depth as vertice i. Furthermore, we denote the set of the ancestors and descendents within k-nearest generations with $\mathbb{A}_i^{(k)}$. Taking vertice 5 in Fig. 6 for example, $\mathbb{A}_5 = \{0, 2, 6, 7, 8, 9, 10\}$, $\mathbb{B}_5 = \{3, 4\}$, and $\mathbb{A}_5^{(1)} = \{2, 6, 7, 8\}$.

After obtaining the spanning tree $\check{\mathscr{G}}_{N+1}$ and the depth of each vertice k denoted by d_k, we can determine the geometry topology of the virtual platoon. In the geometry topology, vehicle i in the virtual platoon will always follow its virtual preceding vehicle P_i indicated by its parent vertice in $\check{\mathscr{G}}_{N+1}$, and will try to keep a desired car-following distance D while tracking the speed of vehicle P_i.

$$\begin{cases} \lim_{t\to\infty}(v_i(t) - v_{P_i}(t)) = 0 \\ \lim_{t\to\infty}(p_i(t) - p_{P_i}(t) - D) = 0 \end{cases}, \quad i \in \mathscr{N}^+ \tag{3}$$

where p_i and v_i are the displacement and speed of vehicle i, respectively, p_{P_i} and v_{P_i} are the displacement and speed of vehicle P_i, respectively. In this case, when the virtual platoon system tends to be stable, the relative motion between any two vehicles i and j are shown in below,

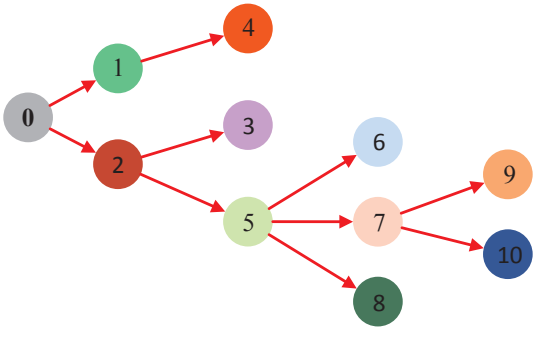

Fig. 6. An example of the spanning tree.

$$\begin{cases} \lim_{t\to\infty}(v_i(t)-v_j(t)) = 0 \\ \lim_{t\to\infty}(p_i(t)-p_j(t)-D(d_i-d_j)) = 0 \end{cases}, \quad \forall\, i,j \in \mathcal{N} \tag{4}$$

When the vehicles i and j have the same depth, we have

$$\lim_{t\to\infty}(p_i(t)-p_j(t)) = 0, \tag{5}$$

which means the vehicles with the same depth in $\mathcal{G}_{N+1}$ will pass the intersection simultaneously. For example, vehicle 3, 4 and 6 in Fig. 6 arrive at the intersection at the same time. We prove that the trajectories of two vehicles with the same depth in $\mathcal{G}_{N+1}$ will not conflict with each other.

Theorem 2. Consider a virtual platoon characterized by $\mathcal{G}_{N+1}$ with the spanning tree $\mathcal{G}_{N+1}$. The trajectories of two vehicles with the same depth in $\mathcal{G}_{N+1}$ have no conflict relationship with each other.

Proof. Suppose that there are N_k vehicles with the same depth k ($\forall\, k$), of which the vertice numbers are n_1, n_2, …, and n_{N_k} ($n_1 < n_2 < \ldots < n_{N_k}$).

For vehicle n_i and n_j ($\forall\, i,j \in \{1, 2, \ldots, N_k\}$):

(1) If $n_j > n_i$, then $n_j \notin \mathbb{P}_{n_i}$.
(2) If $n_j < n_i$ and $n_j \in \mathbb{P}_{n_i}$, then $(n_j, n_i) \in \mathcal{E}_{N+1}$ in $\mathcal{G}_{N+1}$. In this case, according to the proposed search algorithm in Table, vehicle n_i selects the parent vertice with the largest depth in the spanning tree $\mathcal{G}_{N+1}$, which means that the depth of vehicle n_i must be larger than the depth of any parent vertices in $\mathcal{G}_{N+1}$. Hence, $d_{n_i} > d_{n_j}$ in $\mathcal{G}_{N+1}$, which is contradictory with the assumption that vehicle n_i and n_j are with the same depth in $\mathcal{G}_{N+1}$. Consequently, if $n_j < n_i$, then $n_j \notin \mathbb{P}_{n_i}$.

Therefore, for any vehicle n_i and n_j ($\forall\, i,j \in \{1, 2, \ldots, N_k\}$), we have $n_j \notin \mathbb{P}_{n_i}$, which means that the vehicles with the same depth in $\mathcal{G}_{N+1}$ have no conflict with each other. □

Note that the virtual platoon and its geometry topology are only applied in the cooperating zone, while vehicles can follow its proceeding vehicle in the approaching zone. Additionally, when projecting the vehicles, we define the distance as that from the intersection center rather than from the conflict points to ensure that the vehicles with the same depth pass the intersection at the same time. Hence, to ensure the traffic safety, the desired car-following distance must be a little larger because of the definition of the distance, which will indeed reduce the intersection capacity. Therefore, in the proposed method, we sacrifice the traffic efficiency to some extent to guarantee some other important benefits, such as the traffic safety, easy implementation, and low computation complexity.

3.3. Communication topology

It is potential that the performance of distributed control of CAVs at intersections will be maximized when each vehicle obtains the global information, i.e., the motion data of all other vehicles. However, restricted by the communication resources, i.e., bandwidth specifically, the vehicles cannot share information with all the other vehicles. Hence, it is important to model the communication topology and analyze the influence of the communication topology.

The communication aims to share the information of the neighboring vehicles to realize more stable and accurate car following for the virtual platoon. Considering the characteristics of the geometry topology of the virtual platoon, we design two kinds of communication modes, i.e., the communication among vertices with the same depth (Fig. 7(a)) and the communication with ancestor or descendent vertices (Fig. 7(b)). For the latter, the vertice can share information with its ancestor or descendent vertices within k nearest generations. Here, k denotes the communication range, which is limited by communication performance. The information of the vertices with the same depth helps the vertices to keep the consistent position in the virtual platoon and to guarantee simultaneous arrivals at intersections, while the information from ancestors/descendants benefits the car-following performance.

The vertices in $\mathcal{G}_{N+1}$ and information transmission between vertices together make up the communication graph

(a) Communication among the vertices with the same depth

(b) Communication with ancestor or descendent vertices

Fig. 7. Communication modes.

$\overline{\mathrm{G}}_{\mathscr{N}+} = \{\overline{\mathrm{V}}_{\mathscr{N}+}, \overline{\mathrm{E}}_{\mathscr{N}+}\}$. Notice that when the communication range $k > 0$, the spanning tree $\check{\mathscr{G}}_{N+1}$ is a subgraph of the communication graph $\overline{\mathrm{G}}_{\mathscr{N}+}$, since $\overline{\mathrm{G}}_{\mathscr{N}+}$ contains all vertices and edges of $\check{\mathscr{G}}_{N+1}$.

To describe the characteristics of the communication topology, we introduce the adjacency matric $\mathcal{A} = [a_{ij}] \in \mathbb{R}^{N\times N}$ and the pinning matrix $\mathcal{Q} = [q_{ij}] \in \mathbb{R}^{N\times N}$ to represent the communication connection. Specifically,

$$a_{ij} = \begin{cases} 1, & \text{if}(i,j) \in \overline{\mathrm{E}}_{\mathscr{N}+}, \quad i,j \in \mathscr{N}^+ \\ , & \text{else} \end{cases} \tag{6}$$

$$q_{ij} = \begin{cases} 1, & \text{if } i = j \text{ and } (0,i) \in \overline{\mathrm{G}}_{\mathscr{N}+}, \quad i \in \mathscr{N}^+. \\ , & \mathscr{else} \end{cases} \tag{7}$$

Further, the Laplacian matrix $\mathcal{L} = [l_{ij}] \in \mathbb{R}^{N\times N}$ is introduced as

$$l_{ij} = \begin{cases} -a_{ij}, & \text{if } j \neq i \\ \sum\limits_{k\neq i} a_{ik}, & \text{if } j = i, \quad i,j \in \mathscr{N}. \end{cases} \tag{8}$$

Notice that we consider the bidirectional communication, i.e., if $(i,j) \in \overline{\mathrm{E}}_{\mathscr{N}+}$, we have $(j,i) \in \overline{\mathrm{E}}_{\mathscr{N}+}$. Therefore, the adjacency matric $\mathcal{A}$, the pinning matrix $\mathcal{Q}$, and the Laplacian matrix $\mathcal{L}$ are all symmetric matrixes.

Note that the communication topology is dependent on the geometry topology and the global vehicle information is necessary to construct the geometry topology, so the vehicles still need to communicate with a centralized controller in the proposed method. However, the vehicles no longer need to communicate with the centralized controller but with their neighboring vehicles once the geometry topology is determined, which still has potential to decrease the communication load.

3.4. Distributed control

Vehicle dynamics is complex due to numerous nonlinear components such as the engine, transmission, final gear, wheels, and external forces like aerodynamic drag and rolling resistance. By using the feedback linearization technique in the lower controller, the dynamics of a vehicle i can be converted into a linear one as follows (Ploeg et al., 2014):

$$\begin{aligned} &\dot{\boldsymbol{x}}_i(t) = \boldsymbol{A}_i\boldsymbol{x}_i(t) + \boldsymbol{B}_i u_i(t), \\ &\boldsymbol{x}_i(t) = \begin{bmatrix} -p_i \\ v_i \\ a_i \end{bmatrix}, \quad \boldsymbol{A}_i = \begin{bmatrix} 0 & 1 & 0 \\ 0 & 0 & 1 \\ 0 & 0 & -\frac{1}{\tau_i} \end{bmatrix}, \quad \boldsymbol{B}_i = \begin{bmatrix} 0 \\ 0 \\ \frac{1}{\tau_i} \end{bmatrix}, \end{aligned} \tag{9}$$

where p_i, v_i, and a_i are the distance to the intersection center, speed and acceleration, respectively, u_i is the desired acceleration, and τ_i represents the time delay of the vehicle dynamics.

We define the neighborhood set $\mathbb{N}_i$ of vehicle i as the set of vehicles that can communication with vehicle i, i.e.,

$$\mathbb{N}_i = \{j | a_{ij} = 1\} \cup \{0 | q_{ii} = 1\}. \tag{10}$$

According to the geometry topology model, the car following errors between vehicle i and vehicle j are

$$\delta_{\mathrm{p}}^{(i,j)} = p_j(t) - p_i(t) - D(d_j - d_i), \quad \forall\, j \in \mathbb{N}_i. \tag{11}$$

$$\delta_{\mathrm{v}}^{(i,j)} = v_i(t) - v_j(t), \quad \forall\, j \in \mathbb{N}_i. \tag{12}$$

Here, $\delta_{\mathrm{p}}^{(i,j)}$ is the car-following distance error between vehicle i and vehicle j, and $\delta_{\mathrm{v}}^{(i,j)}$ is the car-following speed error between vehicle i and vehicle j.

We use distance error and speed error to construct the linear controller for desired acceleration:

$$\begin{aligned} u_i &= -\sum_{j\in\mathbb{N}_i} k_{p_i}\delta_{\mathrm{p}}^{(i,j)} - \sum_{j\in\mathbb{N}_i} k_{v_i}\delta_{\mathrm{v}}^{(i,j)} \\ &= -k_{p_i}\sum_j a_{ij}(p_j(t) - p_i(t) - D(d_j - d_i)) - k_{p_i}q_{ii}(p_0(t) - p_i(t) - D(d_0 - d_i)) \\ &\quad - k_{v_i}\sum_j a_{ij}(v_i - v_j) - k_{p_i}q_{ii}(v_i - v_0). \end{aligned} \tag{13}$$

Here, k_{p_i} and k_{v_i} are the feedback gains of distance error and speed error, respectively, and u_i is the controller input, i.e., the desired acceleration of vehicle i.

By introducing the car following model, we set the car-following errors between the virtual leading vehicle 0 and vehicle i as the new state variables $\overline{\boldsymbol{x}}_i$ of vehicle i, i.e.,

$$\overline{\boldsymbol{x}}_i = \begin{bmatrix} \overline{x}_{i,1} \\ \overline{x}_{i,2} \\ \overline{x}_{i,3} \end{bmatrix} = \begin{bmatrix} p_0 - p_i - D(d_0 - d_i) \\ v_i - v_0 \\ a_i \end{bmatrix}, \quad \forall\, i \in \{1,\, 2,\, \cdots, N\}, \tag{14}$$

and maintain the controller input of vehicle i, i.e., $\overline{u}_i = u_i$.

Hence, the car-following dynamic model is

$$\dot{\overline{\boldsymbol{x}}}_i = \boldsymbol{A}_i \overline{\boldsymbol{x}}_i + \boldsymbol{B}_i \overline{u}_i, \quad \forall\, i \in \{1,\, 2,\, \cdots, N\}. \tag{15}$$

Besides, the linear feedback law can be simplified to

$$\overline{u}_i = -k_{p_i} \sum_j (l_{ij} + q_{ij}) \overline{x}_{j,1} - k_{v_i} \sum_j (l_{ij} + q_{ij}) \overline{x}_{j,2}. \tag{16}$$

Let $\boldsymbol{k}_i = [k_{p_i},\, k_{v_i},\, 0]^T$, we have

$$\overline{u}_i = -\sum_j (l_{ij} + q_{ij}) \boldsymbol{k}^T \overline{\boldsymbol{x}}_j, \quad \forall\, i \in \{1,\, 2,\, \cdots, N\}. \tag{17}$$

3.5. Stability analysis

In this paper, we consider homogeneous vehicle platoon, so we assume that the time delay of all vehicles are the same, i.e., $\tau_i = \tau$, which means $\boldsymbol{A}_i = \boldsymbol{A}$ and $\boldsymbol{B}_i = \boldsymbol{B}$. Additionally, the control law of all vehicles are the same, i.e., $\boldsymbol{k}_i = [k_{p_i},\, k_{v_i},\, 0]^T = [k_p,\, k_v,\, 0]^T = \boldsymbol{k}$. Note that this assumption is not realistic, but it is a common assumption for the platoon control (Li et al., 2017; Zheng et al., 2016a, 2016b). Additionally, we will also study the intersection management for heterogeneous vehicle dynamics and controllers in future work.

Given the aggregated system state $\boldsymbol{X} = [\overline{\boldsymbol{x}}_1^T, \overline{\boldsymbol{x}}_2^T, \cdots, \overline{\boldsymbol{x}}_N^T]^T$ and the aggregated system input $\boldsymbol{U} = [\overline{u}_1, \overline{u}_2, \cdots, \overline{u}_N]^T$, the system dynamics can be expressed as

$$\dot{\boldsymbol{X}} = \overline{\boldsymbol{A}}\boldsymbol{X} + \overline{\boldsymbol{B}}\boldsymbol{U}, \tag{18}$$

$$\boldsymbol{U} = -\overline{\boldsymbol{C}}\boldsymbol{X}.$$

where

$$\overline{\boldsymbol{A}} = \begin{bmatrix} \boldsymbol{A} & & & \\ & \boldsymbol{A} & & \\ & & \ddots & \\ & & & \boldsymbol{A} \end{bmatrix} = \boldsymbol{I}_N \otimes \boldsymbol{A} \in \mathbb{R}^{3N \times 3N}, \tag{19}$$

$$\overline{\boldsymbol{B}} = \begin{bmatrix} \boldsymbol{B} & & & \\ & \boldsymbol{B} & & \\ & & \ddots & \\ & & & \boldsymbol{B} \end{bmatrix} = \boldsymbol{I}_N \otimes \boldsymbol{B} \in \mathbb{R}^{3N \times N}, \tag{20}$$

$$\overline{\boldsymbol{C}} = \begin{bmatrix} (l_{11} + q_{11})\boldsymbol{k}^T & (l_{12} + q_{12})\boldsymbol{k}^T & \cdots & (l_{1N} + q_{1N})\boldsymbol{k}^T \\ (l_{21} + q_{21})\boldsymbol{k}^T & (l_{22} + q_{22})\boldsymbol{k}^T & \cdots & (l_{2N} + q_{2N})\boldsymbol{k}^T \\ \vdots & \vdots & \ddots & \vdots \\ (l_{N1} + q_{N1})\boldsymbol{k}^T & (l_{N2} + q_{N2})\boldsymbol{k}^T & \cdots & (l_{NN} + q_{NN})\boldsymbol{k}^T \end{bmatrix} = (\mathcal{L} + Q) \otimes \boldsymbol{k}^T \in \mathbb{R}^{N \times 3N}, \tag{21}$$

Here, $\boldsymbol{I}_N$ denotes the N by N identical matrix, and $\otimes$ denotes Kronecker product, i.e.,

$$A \otimes B = \begin{bmatrix} a_{11}B & \cdots & a_{1n}B \\ \vdots & \ddots & \vdots \\ a_{m1}B & \cdots & a_{mn}B \end{bmatrix} \in \mathbb{R}^{mp \times nq}, \tag{22}$$

where $A \in \mathbb{R}^{m \times n}$, $B \in \mathbb{R}^{p \times q}$.

Consequently, the system dynamics equation can be written as

$$\dot{\boldsymbol{X}} = (\boldsymbol{I}_N \otimes \boldsymbol{A} - (\mathcal{L} + Q) \otimes \boldsymbol{B}\boldsymbol{k}^T)\boldsymbol{X}. \tag{23}$$

Here, $\boldsymbol{A}$ and $\boldsymbol{B}$ reflect the characteristics of the vehicle dynamics, $\boldsymbol{X}$ indicates the no-conflict geometry topology of the virtual platoon, $\mathcal{L}$ and Q express the communication structure, and $\boldsymbol{k}$ displays the feedback controller.

The most primary purpose of controller design is to ensure the closed-loop stability. For (23), the stability can be guaranteed by properly choosing the feedback gains $\boldsymbol{k}^T$ so that all the eigenvalues of $\boldsymbol{I}_N \otimes \boldsymbol{A} - (\mathcal{L} + Q) \otimes \boldsymbol{B}\boldsymbol{k}^T$ are negative.

Lemma 1. Consider a matrix $\mathcal{M} = [m_{ij}] \in \mathbb{R}^{N \times N}$ and a set $J = \{i \in \{1,\, 2,\, ...,N\} || m_{ii}| > \sum_{i=1, j \neq i}^{n} |m_{ij}|\} \neq \varnothing$. $\mathcal{M}$ is nonsingular, if $\forall\, i \notin J$ there exists a nonzero sequence $\{m_{ii_1},\, m_{i_1 i_2},\, ...,m_{i_r j}\}$ in $\mathcal{M}$ with $j \in J$.

Theorem 3. The eigenvalues of the matrix $(\mathcal{L} + Q)$ are real and positive when the communication range $k \geq 1$.

Proof. Firstly, since $\mathcal{L}$ and Q are both real symmetric matrixs, we know that $\mathcal{L}+Q$ is also real and symmetric. Hence, the eigenvalues of matrix $\mathcal{L}+Q$ are real.

Secondly, according to Gerschgorin's disk Theorem (Zheng et al., 2016a), all the eigenvalues of $\mathcal{L}+Q$ denoted by λ satisfy the inequation below:

$$|\lambda - l_{ii} - q_{ii}| \leqslant \sum_{j=1, j\neq i}^{N} |l_{ij}|, \quad \forall\, i \in \mathcal{N}.$$

Besides, since $\sum_{j=1,j\neq i}^{N} |l_{ij}| = \sum_{j=1,j\neq i}^{N} |a_{ij}| = l_{ii} \leqslant l_{ii} + q_{ii} (> 0)$, we know that $|\lambda - (l_{ii}+q_{ii})| \leqslant l_{ii}+q_{ii}$, which means $\lambda \geqslant 0$. Therefore, $\mathcal{L}+Q$ is positive semi-definite.

Finally, we prove that $\mathcal{L}+Q$ is nonsingular.

From Section 3.3 we know that there exist the paths from vertice 0 to any other vertices in $\overline{\mathrm{G}}_{\mathcal{N}+}$. Hence, for these vertices without the edge with vertice 0 in $\overline{\mathrm{G}}_{\mathcal{N}+}$, i.e., $\forall\, i \in \{i | q_{ii} = 0\}$, there must exist a path $\{(0, j), (j, i_r), \ldots, (i_1, i)\}$ in $\overline{\mathrm{G}}_{\mathcal{N}+}$, which means that $\{a_{ii_1}, a_{i_1 i_2}, \ldots, a_{i_r j}\} \neq 0$ and $q_{jj} > 0$. Considering $-a_{mn} = l_{mn} = l_{mn} + q_{mn} (m \neq n)$, we have that $\forall\, i \in \{i | q_{ii} = 0\}$, there exists a nonzero sequence $\{l_{ii_1} + q_{ii_1}, l_{i_1 i_2} + q_{i_1 i_2}, \ldots, l_{i_r j} + q_{i_r j}\}$.

Let $J = \{i \in \{1, 2, \ldots, N\} | |l_{ii} + q_{ii}| > \sum_{i=1, j\neq i}^{N} |l_{ij} + q_{ij}|\}$. Since $|l_{ii} + q_{ii}| = \sum_{i=1,j\neq i}^{N} a_{ij} + q_{ii}$ and $\sum_{i=1,j\neq i}^{N} |l_{ij} + q_{ij}| = \sum_{i=1,j\neq i}^{N} |l_{ij}| = \sum_{i=1,j\neq i}^{N} a_{ij}$, we have $J = \{i \in \{1, 2, \ldots, N\} | q_{ii} > 0\}$. Therefore, $i \notin J \Leftrightarrow i \in \{i | q_{ii} = 0\}$. Hence, $\forall\, i \notin J$, $\exists\, j \in J$, there exists a nonzero sequence $\{l_{ii_1} + q_{ii_1}, l_{i_1 i_2} + q_{i_1 i_2}, \ldots, l_{i_r j} + q_{i_r j}\}$ in $\mathcal{L}+Q$. According to ***Lemma* 1**, we know that $\mathcal{L}+Q$ is nonsingular.

In conclusion, all the eigenvalues of $\mathcal{L}+Q$ are real and positive. □

There exists an invertible matrix $\boldsymbol{P}$ so that $\mathcal{L}+Q$ can be transformed to Jordan normal form using it:

$$\boldsymbol{P}^{-1}(\mathcal{L}+Q)\boldsymbol{P} = \boldsymbol{J} = \begin{bmatrix} \boldsymbol{J}_1 & & & \\ & \boldsymbol{J}_2 & & \\ & & \ddots & \\ & & & \boldsymbol{J}_r \end{bmatrix},$$

where $\boldsymbol{J}_i$ is a Jordan block with dimensions of $n_i \times n_i$.

We conduct the similarity transformation for $\boldsymbol{I}_N \otimes \boldsymbol{A} - (\mathcal{L}+Q) \otimes \boldsymbol{B}\boldsymbol{k}^T$ using $\boldsymbol{P}$ and $\boldsymbol{P}^{-1}$:

$$(\boldsymbol{P} \otimes \boldsymbol{I}_N)^{-1}(\boldsymbol{I}_N \otimes \boldsymbol{A} - (\mathcal{L}+Q) \otimes \boldsymbol{B}\boldsymbol{k}^T)(\boldsymbol{P} \otimes \boldsymbol{I}_N) = \boldsymbol{I}_N \otimes \boldsymbol{A} - \boldsymbol{J} \otimes (\boldsymbol{B}\boldsymbol{k}^T).$$

Here $\boldsymbol{I}_N \otimes \boldsymbol{A} - \boldsymbol{J} \otimes (\boldsymbol{B}\boldsymbol{k}^T)$ is a block upper triangular matrices and has the same characteristic equation as $\boldsymbol{I}_N \otimes \boldsymbol{A} - (\mathcal{L}+Q) \otimes \boldsymbol{B}\boldsymbol{k}^T$. Therefore, the characteristic equation of $\boldsymbol{I}_N \otimes \boldsymbol{A} - (\mathcal{L}+Q) \otimes \boldsymbol{B}\boldsymbol{k}^T$ is

$$|\lambda \boldsymbol{I}_{3N} - (\boldsymbol{A} - \boldsymbol{J} \otimes (\boldsymbol{B}\boldsymbol{k}^T))| = \prod_{i=1}^{r} |\lambda \boldsymbol{I}_3 - \boldsymbol{A} + \lambda_i \boldsymbol{B}\boldsymbol{k}^T|^{n_i} = 0, \tag{24}$$

where $\boldsymbol{I}_{3N}$ denotes the $3N$ by $3N$ identical matrix.

We have

$$|\lambda \boldsymbol{I}_3 - \boldsymbol{A} + \lambda_i \boldsymbol{B}\boldsymbol{k}^T| = \lambda^3 + \frac{\lambda^2}{\tau} + \frac{k_v \lambda_i \lambda}{\tau} + \frac{k_p \lambda_i}{\tau} = 0. \tag{25}$$

According to Routh–Hurwitz stability criterion, the necessary and sufficient conditions for the stability of the closed-loop systems are

$$\frac{k_v \lambda_i}{\tau} > 0, \quad -\frac{k_p \lambda_i}{\tau} > 0, \quad \frac{k_v \lambda_i}{\tau} \cdot \frac{1}{\tau} + \frac{k_p \lambda_i}{\tau} > 0.$$

Since all the eigenvalues λ_i of $\mathcal{L}+Q$ are real and positive, the necessary and sufficient conditions for platoon stability are

$$k_p > 0, \quad k_v > k_p \tau. \tag{26}$$

These conditions are consistent with Zheng et al. (2016b). From (26), we can see that the computation of the feedback control law is independent of the size of the virtual platoon. Hence, the proposed method is able to organize the vehicle motion with genuine distributed control.

Remark. The proposed method consists of 3 steps: firstly, to construct the conflict-free geometry topology; secondly, to obtain the motion information from the neighbored vehicles via V2V communication; thirdly, to conduct the linear feedback control, which is independent of the size of the virtual platoon. For the first step, the time complexity of the projection and sort algorithm to construct the virtual platoon is $O(n^2)$ and the time complexity of the search algorithm in Table 1 is also $O(n^2)$, where n is the size of the virtual platoon. Therefore, computation complexity of the proposed method is $O(n^2)$ which is really computational efficient.

4. Numerical test and result

To verify the proposed distributed control method, we conduct the numerical test. We consider the typical intersection shown in

Table 2
Parameters.

Scenario Parameters	The radius of the overall intersection	d_i	250 m
	The radius of the cooperating zone	d_c	200 m
Controller Parameters	Feedback gain for distance error	k_p	0.15
	Feedback gain for speed error	k_v	0.7
	Desired speed of the virtual leading vehicle	v_t	10 m/s
	Desired car-following distance	D	25 m
	Minimal speed	v_{min}	0 m/s
	Maximal speed	v_{max}	20 m/s
	Minimal acceleration	a_{min}	-3 m/s^2
	Maximal acceleration	a_{max}	1.5 m/s^2
Simulation Parameters	Average time headway	–	3 s
	Average initial speed	–	10 m/s

Fig. 1. The vehicles arrived at the intersection entrances randomly. The vehicles' arrivals obey a Poisson distribution with the average time headway 6 s, and the vehicles' initial speeds obey a Gaussian distribution with the average speed 10 m/s. When the vehicles enter into the cooperating zone, they share the information with each other, coordinate the movements of themselves using the no-conflict distributed controllers, and go through the intersection orderly. The main parameters of the simulation and the controller are shown in Table 2. The total simulation time was 1 h and 2436 vehicles participated in the simulation.

In the simulation, we count the total computation time of the geometry topology construction of the virtual platoon and the control input calculation of a single vehicle, of which the results show that the average and maximum time costs on computation are 0.0036 s and 0.0078 s, respectively, which proves the low computation complexity of the proposed method. During the simulation, all vehicles passed the intersection orderly and without any potential collision. Some validation results, including the vehicle, speed, and acceleration profiles, are exhibited in Fig. 8 where the horizontal axes represent the vehicle locations, i.e., the corresponding approaching entrances and the distance to the intersection, and the vertical axes represent the time, speed and acceleration, respectively. From Fig. 8(a), we can see that the vehicles from different entrances pass the intersection orderly and uniformly. Some vehicles pass the intersection at the same time but they are conflict-free, which will be illustrated in Fig. 9 in detail. Figs. 8(b) and 8(c) show that the vehicles adjust their speed and acceleration once they enter the cooperating zone, and they rapidly reach the steady states with a consensus and stable speed.

Fig. 9 presents the intersection arrival time of approaching vehicles in different traffic movements. The circle contours represent the different levels of arrival times of which the values are shown in the color bar of the figure. The arrows denote different vehicle movements. The points mean the vehicles' arrival time at the intersection. The points on the same circle correspond to vehicles going through the intersection at the same time. From the figure, we can see that the vehicles passing the intersection simultaneously have no conflicting relationship with each other, which proves that our method has the ability to coordinate the vehicle passing the intersection with conflict-free movements. For example, vehicle 22, vehicle 23, and vehicle 24 locate in the circle of 53.5 s and their movements are eastbound right, westbound right, and southbound right, which do not conflict at the intersection obviously.

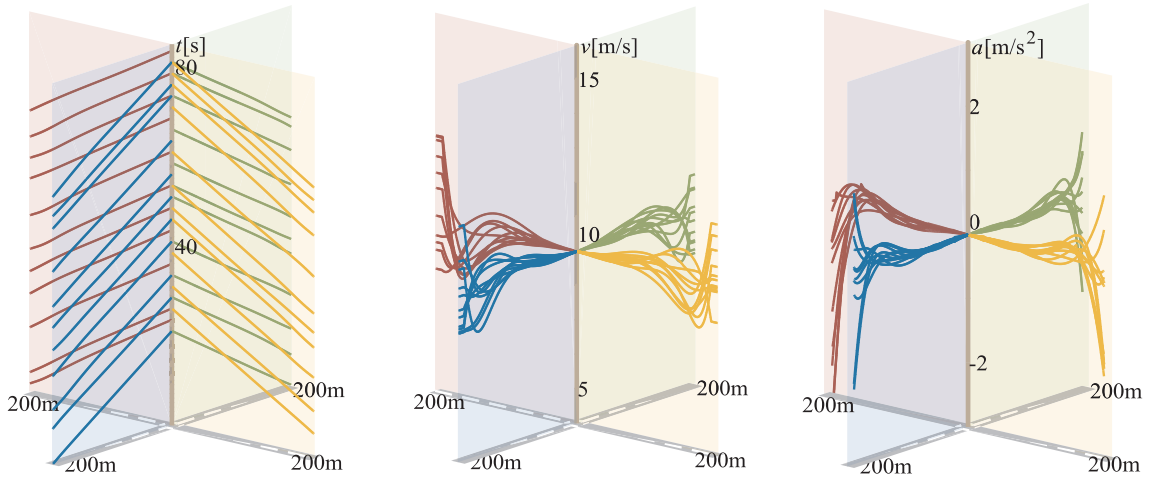

(a) Position Profiles (b) Speed Profiles (c) Acceleration Profiles

Fig. 8. Motion of approaching vehicles.

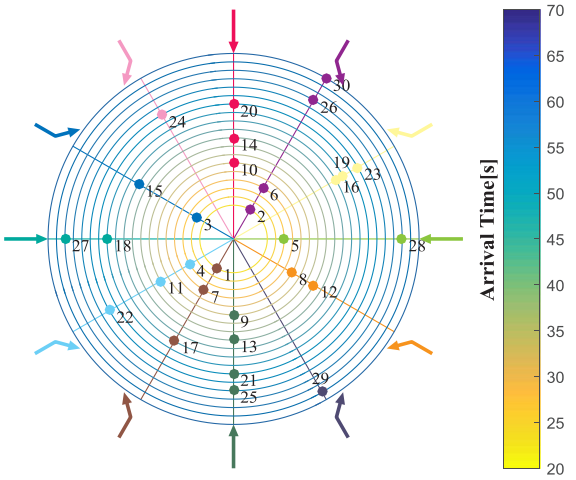

Fig. 9. Arrival time of approaching vehicles.

5. Conclusion and discussion

This paper proposed a distributed conflict-free cooperation method for multiple connected and automated vehicles at an unsignalized intersection. We built the conflict model of traffic movements. By adopting the rotating projection, we transformed the 2-dimension vehicle cluster at the intersection to a 1-dimension virtual platoon in a virtual lane. The vehicle conflict directed graph and its spanning tree were demonstrated to reconstruct the platoon geometry topology and obtain a new virtual platoon geometry structure which was theoretically proved to be conflict-free. Based on the characteristics of the geometry structure, the communication topology including two communication modes was introduced to enhance car-following performance for the virtual platoon. The linear feedback controller was presented and the aggregate dynamics model of the virtual platoon was suggested based on the geometry topology, communication topology, vehicle dynamics, and the distributed controller. Using the matrix decomposition, we found the necessary and sufficient conditions of the system stability, which support the distributed controller design. The validation results prove that the proposed distributed conflict-free cooperation method is able to organize the movements of the approaching vehicles effectively without movement conflicts.

We illustrated our distributed conflict-free cooperation method at a typical intersection with four entrances, four exits and one lane in each entrance or exit, but this method also adapts to other types of intersections, regardless of the channelization and the geometry form of the intersection, once the traffic movements and their conflict relationship can be determined. This method has potential to promote a new unsignalized way of traffic control for connected and automated vehicles.

Unsolved topics for future research include the distributed control for the heterogeneous vehicle cluster at the intersection, and vehicle conflict-free control at a road network which consists of multiple unsignalized intersections.

Acknowledgment

Biao Xu and Shengbo Eben Li are contributed equally to this paper. This study is supported by NSF China with 51575293, 51622504 and 51605245, National Key R&D Program of China with 2016YFB0100906, and International Sci&Tech Cooperation Program of China under 2016YFE0102200.

Appendix A. Supplementary material

Supplementary data associated with this article can be found, in the online version, at http://dx.doi.org/10.1016/j.trc.2018.06.004.

References

Ahmane, M., Abbas-Turki, A., Perronnet, F., Wu, J., El Moudni, A., Buisson, J., Zeo, R., 2013. Modeling and controlling an isolated urban intersection based on cooperative vehicles. Transp. Res. Part C: Emerg. Technol. 28, 44–62.

Chen, L., Englund, C., 2016. Cooperative intersection management: a survey. IEEE Trans. Intell. Transp. Syst. 17 (2), 570–586.

Choi, E.H., 2010. Crash factors in intersection-related crashes: an on-scene perspective (No. HS-811 366).

Dai, P., Liu, K., Zhuge, Q., Sha, E.H.M., Lee, V.C.S., Son, S.H., 2016. Quality-of-experience-oriented autonomous intersection control in vehicular networks. IEEE Trans. Intell. Transp. Syst. 17 (7), 1956–1967.

Dresner, K., Stone, P., 2008. A multiagent approach to autonomous intersection management. J. Artif. Intell. Res. 31, 591–656.

Fax, J.A., Murray, R.M., 2004. Information flow and cooperative control of vehicle formations. IEEE Trans. Autom. Control 49 (9), 1465–1476.

Feng, Y., Head, K., K. L., Khoshmagham, S., & Zamanipour, M., 2015. A real-time adaptive signal control in a connected vehicle environment. Transp. Res. Part C: Emerg. Technol. 55, 460–473.

Goodall, N., Smith, B., Park, B., 2013. Traffic signal control with connected vehicles. Transp. Res. Rec J. Transp. Res. Board 2381, 65–72.
Huang, S., Sadek, A.W., Zhao, Y., 2012. Assessing the mobility and environmental benefits of reservation-based intelligent intersections using an integrated simulator. IEEE Trans. Intell. Transp. Syst. 13 (3), 1201–1214.
Kamal, M.A.S., Imura, J.I., Hayakawa, T., Ohata, A., Aihara, K., 2015. A vehicle-intersection coordination scheme for smooth flows of traffic without using traffic lights. IEEE Trans. Intell. Transp. Syst. 16 (3), 1136–1147.
Lewis, F.L., Zhang, H., Hengster-Movric, K., Das, A., 2013. Cooperative Control of Multi-agent Systems: Optimal and Adaptive Design Approaches. Springer Science & Business Media.
Lee, J., Park, B., 2012. Development and evaluation of a cooperative vehicle intersection control algorithm under the connected vehicles environment. IEEE Trans. Intell. Transp. Syst. 13 (1), 81–90.
Lee, J., Park, B.B., Malakorn, K., So, J.J., 2013. Sustainability assessments of cooperative vehicle intersection control at an urban corridor. Transp. Res. Part C: Emerg. Technol. 32, 193–206.
Li, L., Wang, F.Y., 2006. Cooperative driving at blind crossings using intervehicle communication. IEEE Trans. Veh. Technol. 55 (6), 1712–1724.
Li, Z., Duan, Z., Chen, G., Huang, L., 2010. Consensus of multiagent systems and synchronization of complex networks: a unified viewpoint. IEEE Trans. Circuits Syst. I Regul. Pap. 57 (1), 213–224.
Li, S.E., Qin, X., Li, K., Wang, J., Xie, B., 2017. Robustness analysis and controller synthesis of homogeneous vehicular platoons with bounded parameter uncertainty. IEEE/ASME Trans. Mechatron. 22 (2), 1014–1025.
Naus, G.J., Vugts, R.P., Ploeg, J., van de Molengraft, M.J., Steinbuch, M., 2010. String-stable CACC design and experimental validation: a frequency-domain approach. IEEE Trans. Veh. Technol. 59 (9), 4268–4279.
Ploeg, J., Shukla, D.P., van de Wouw, N., Nijmeijer, H., 2014. Controller synthesis for string stability of vehicle platoons. IEEE Trans. Intell. Transp. Syst. 15 (2), 854–865.
Roess, R.P., Prassas, E.S., McShane, W.R., 2011. Traffic engineering, third ed. Prentice-Hall, Englewood Cliffs, NJ, USA.
Seiler, P., Pant, A., Hedrick, K., 2004. Disturbance propagation in vehicle strings. IEEE Trans. Autom. Control 49 (10), 1835–1842.
Tarjan, R., 1972. Depth-first search and linear graph algorithms. SIAM J. Comput. 1 (2), 146–160.
Wang, X., Saberi, A., Stoorvogel, A.A., Grip, H.F., Yang, T., 2013. Consensus in the network with uniform constant communication delay. Automatica 49 (8), 2461–2467.
Wu, J., Abbas-Turki, A., El Moudni, A., 2012. Cooperative driving: an ant colony system for autonomous intersection management. Appl. Intell. 37 (2), 207–222.
Xiao, L., Gao, F., 2011. Practical string stability of platoon of adaptive cruise control vehicles. IEEE Trans. Intell. Transp. Syst. 12 (4), 1184–1194.
Xu, B., Ban, X. J., Bian, Y., Wang, J., Li, K., 2017. V2I based cooperation between traffic signal and approaching automated vehicles. In: 2017 IEEE Intelligent Vehicles Symposium (IV), IEEE, pp. 1658–1664.
You, K., Xie, L., 2011. Network topology and communication data rate for consensusability of discrete-time multi-agent systems. IEEE Trans. Autom. Control 56 (10), 2262–2275.
Zhou, J., Peng, H., 2005. Range policy of adaptive cruise control vehicles for improved flow stability and string stability. IEEE Trans. Intell. Transp. Syst. 6 (2), 229–237.
Zhang, K., Zhang, D., de La Fortelle, A., Wu, X., Gregoire, J., 2015. State-driven priority scheduling mechanisms for driverless vehicles approaching intersections. IEEE Trans. Intell. Transp. Syst. 16 (5), 2487–2500.
Zheng, Y., Li, S.E., Wang, J., Cao, D., Li, K., 2016a. Stability and scalability of homogeneous vehicular platoon: Study on the influence of information flow topologies. IEEE Trans. Intell. Transp. Syst. 17 (1), 14–26.
Zheng, Y., Li, S.E., Li, K., Wang, L.Y., 2016b. Stability margin improvement of vehicular platoon considering undirected topology and asymmetric control. IEEE Trans. Control Syst. Technol. 24 (4), 1253–1265.